Journal of The Electrochemical Society, **154** (12) B1295-B1304 (2007)
0013-4651/2007/154(12)/B1295/10/$20.00 © The Electrochemical Society

Validated Leverett Approach for Multiphase Flow in PEFC Diffusion Media

I. Hydrophobicity Effect

E. C. Kumbur,* K. V. Sharp, and M. M. Mench,z**

Fuel Cell Dynamics and Diagnostics Laboratory, Department of Mechanical and Nuclear Engineering, The Pennsylvania State University, University Park, Pennsylvania 16802, USA

This is the first in a series of papers in which we introduce a validated Leverett function appropriate for SGL 24 series carbon paper fuel cell diffusion media (DM) that describes the capillary pressure as a function of liquid saturation and hydrophobic additive content. The presented relationship was derived based on the benchmark data gathered from direct measurements of drainage capillary pressure-saturation of differently engineered DM (coated with a microporous layer) tailored with various poly(tetrafluoroethylene) content (ranging from 5 to 20 wt %) at room temperature under no compression. A key feature of the relationship is that the contact angle is implicitly embedded into the hydrophobicity parameter, thereby eliminating any ambiguity regarding the selection of a representative surface contact angle. A detailed comparative analysis of the present Leverett function and the standard Leverett function with the experimental data was performed. The standard Leverett function is found to exhibit significant deviation from the experimental data, whereas the present empirical function successfully predicts the capillary pressure over the entire saturation domain. Finally, additional spontaneous capillary imbibition experiments were performed to obtain estimates for the water retention capacity of a typical fuel cell DM as a function of the hydrophobicity of bilayered DM.
 [DOI: 10.1149/1.2784283]

Manuscript submitted March 28, 2007; revised manuscript received August 10, 2007. Available electronically October 16, 2007.

Fuel cells offer the possibility of a low-emission power source for automotive, stationary, and portable applications but face a number of technical challenges that must be surmounted in order to successfully compete against internal combustion (IC) engines and batteries. Among those, water management is a major bottleneck not only for efficient fuel cell operation, but also for operational stability and durability under normal and cold-start operations.[1-5] The proper engineering of fuel cell materials may lead to an optimized water balance, increasing power, and durability. However, the prediction of material design and microfluidic management are currently hindered by the lack of fundamental understanding of the proper transport relationships governing the multiphase flow in the porous diffusion media (DM) and catalyst layer. There is also a paucity of experimental data and analysis in the existing literature necessary for guiding the engineering of fuel cell DM materials with favorable internal architectures.

Many studies[6-8] reveal that liquid water transport is a dominating factor influencing the performance of the fuel cell and is closely related to the capillary transport characteristics of thin-film fuel cell DM. Therefore, the morphological characteristics of a bilayered DM, along with the localized anisotropic nature of transport parameters, should be well known in order to establish an accurate physical theory of capillary transport in these materials. Nearly every multiphase transport model requires the specific capillary pressure-saturation relationship of fluid and porous medium to correlate the capillary pressure as a function of saturation, wettability, and other material properties. Unfortunately, the science of multiphase transport through the thin-film DM tailored with mixed wettability is not well developed, yet much of the present level of understanding is based on application of porous media theory from civil and petroleum engineering studies of fluid flow through packed soil beds with uniform wettability.

In most fuel cell models, the common approach to simulate the capillary transport in these porous materials relies on the semiempirical correlation proposed for soil beds with uniform wettability by Leverett[9] and Udell.[10] Pasaogullari and Wang[11] and Nam and Kaviany[12] proposed the calibrated version of the Leverett *J*-function to account for the hydrophobic characteristics of the fuel cell DM. Even though the classical Leverett approach serves as a useful starting point to model the liquid transport in the porous DM, the direct application of Udell's sand-based relationship has been determined to be insufficient to accurately describe the capillary pressure-saturation relationship in typical fuel cell DM.[1] The ineffectiveness of the traditional approach for fuel cell DM potentially stems from the fact that the fuel cell porous media, including the catalyst layer and DM, are actually a heterogeneous mixture of various components. This heterogeneous composition represents a class of materials with mixed wettability and has not been previously treated by soil science. Additionally, the effects of assembly compression, amount of hydrophobic loading, and operating temperature on the capillary transport characteristics have not yet been adequately assessed and therefore should be considered to fully elucidate the capillary transport mechanism in these thin-film porous media. Relationships governing the multiphase transport are needed for application to these thin-film materials to enable well-defined microfluidic management and provide the necessary guidance for engineering fuel cell materials.

Acknowledging the existence of minute length scale and the presumed anisotropic nature of the thin-film porous DM, many studies[13-17] have focused on bulk material optimization of the DM, neglecting the complex interaction of the material properties and transport phenomena. Several studies[18,19] investigated the morphological properties of the porous DM. The porosity and total pore distribution of several DM measured using the mercury intrusion technique were reported,[18,19] even though the mercury intrusion technique is incapable of distinguishing the hydrophobic and hydrophilic pore distribution of DM and requires high pressures (more than 100 atm), which can lead to a substantial deformation of the DM structure. Due to these inherent limitations of the mercury intrusion technique, these studies were limited to qualitatively explaining polymer electrolyte fuel cell (PEFC) performance on the basis of observed DM morphological features. Recently, Gostick et al.[20] reported an experimental approach for determining the dependence of capillary pressure on wetting phase saturation along a desaturation path (drainage) for various DM. The dual pore distribution (hydrophobic and hydrophilic) of several DM was obtained.[20] However, no benchmark relationships relating the tailored material and geometric properties of the DM with the multiphase flow parameters were explicitly developed.

Recognizing the experimental limitations associated with the complex nature of DM, the development of approximate mathematical models is imperative to the understanding and prediction of mul-

* Electrochemical Society Student Member.
** Electrochemical Society Active Member.
z E-mail: mmm124@psu.edu

Table I. Material properties of the tested DM samples.[a]

Material	Type	Thickness (μm)	PTFE Macro-substrate (wt %)	Porosity	Permeability (cm^3/cm^2 s)
SGL 24BC	Paper w/MPL	235	5	0.76	0.60
SGL 24CC	Paper w/MPL	235	10	0.75	0.60
SGL 24DC	Paper w/MPL	235	20	0.75	0.45
E-TEK ELAT 1200W	Cloth w/MPL	275	>20	N/A	>8.00

[a] All values are adapted from manufacturer technical specification sheets. Note that the values of porosity, permeability, and PTFE content given above represent the material properties of the tested macro fuel cell diffusion media substrate (i.e., macro DM without MPL).

tiphase transport phenomenon in the DM. An excellent review of the recent modeling efforts and the current challenges are provided by Djilali et al.[21] However, the accuracy of the existing modeling efforts is inherently limited due to the scarcity of experimental data representing the accurate capillary transport physics in porous fuel cell DM.

The present study is motivated by the need to develop an appropriate Leverett function that precisely describes the capillary pressure-saturation relationship of fuel cell porous DM with mixed wettability. The effects of degree of mixed wettability on the capillary transport and the morphological characteristics of a fuel cell DM have been thoroughly investigated at room temperature under no compression. A validated Leverett-type empirical function is deduced from a wide range of drainage capillary pressure-saturation measurements of the commercially available SGL series bilayered DM (with microporous layer) treated with various degrees of PTFE loadings (from 5 to 20 wt %). Additionally, the accuracy of the commonly used Leverett function and the present empirical correlation was analyzed by comparison with the experimental data.

Method of Approach

Diffusion media samples.— The thin-film fuel cell DM utilized in the present study are constructed from a sheet of electrically conductive macroporous substrate with varying degree of mixed wettability, such as a nonwoven carbon paper or a woven carbon cloth, both of which are coated with a microporous layer on one side.

In order to elucidate the structural variation between the carbon paper and cloth, both SGL 24 series (SIGRACET gas diffusion layers) carbon paper and E-TEK Elat 1200W carbon cloth were investigated. The DM samples tested are commonly used in various fuel cell applications and were designed for a wide range of operating conditions. In terms of morphological structure, both carbon paper and cloth have heterogeneous structure with pore size ranging from a few micrometers to tens of micrometers. The porosities range from 70 to 90%, whereas the thickness varies from 200 to 300 μm. These naturally hydrophilic DM are typically tailored during processing by addition of hydrophobic material poly(tetrafluoroethylene) (PTFE), known as Teflon, to improve the liquid water transport. An additional thin microporous layer (MPL) of carbon black mixed with PTFE is also introduced on one side of the DM substrate to provide better electrical contact with the catalyst layer and reduce the water saturation in the macroporous substrate.[7]

The material properties of the DM samples, as supplied by the manufacturers, are provided in Table I. In the present study, SGL 24BC (5 wt % PTFE content), SGL 24CC (10 wt % PTFE content), and SGL 24DC (20 wt % PTFE content) from SGL 24 carbon paper series, and E-TEK Elat 1200W carbon cloth (nonuniform PTFE content >20% wt %) were included in the experimental matrix in order to cover the possible hydrophobic treatment range and woven or nonwoven characteristic of the DMs that are typically used in fuel cell applications. Figure 1 shows scanning electron microscopy (SEM) images of the structure of the selected carbon cloth and carbon papers.

Experimental approach.— Capillary pressure-saturation measurements were performed using the method of standard porosimetry (MSP) technique developed by Porotech, Ltd. This technique is based on the capillary equilibrium principle, providing a means of nondestructive measurement of the capillary pressure-saturation curves in porous materials.[22] A descriptive schematic of the technique is illustrated in Fig. 2. The DM samples were placed in capillary contact between two standard samples having a known capillary pressure-saturation curve, one of which was placed at the open surface of the stack (where the liquid evaporates) and the other at the closed surface. The standard sample was chosen such that its pore size is in the range of the typical fuel cell DM.[22] Different liquids were utilized as working fluids to evaluate the mixed wettability characteristics of DMs. Highly wetting liquid octane was used as a working liquid to determine the *overall pore distribution*, whereas deionized water allowed for the determination of the *hydrophilic pore network* because it is naturally imbibed only by the hydrophilic pores.

Periodically, a small portion of the liquid was slowly evaporated by a flow of dry inert gas while the standard sample and tested DM were kept in capillary contact to allow the establishment of a new capillary equilibrium. At each equilibrium, the mass of each sample was measured to obtain the wetting phase saturations, enabling the determination of the corresponding capillary pressure of the standard sample from its known characteristics.[22] In capillary equilibrium, this pressure is equal to the capillary pressure of the fuel cell DM sample. This process was continuously repeated until most of the liquid had evaporated from the test samples.[20,22]

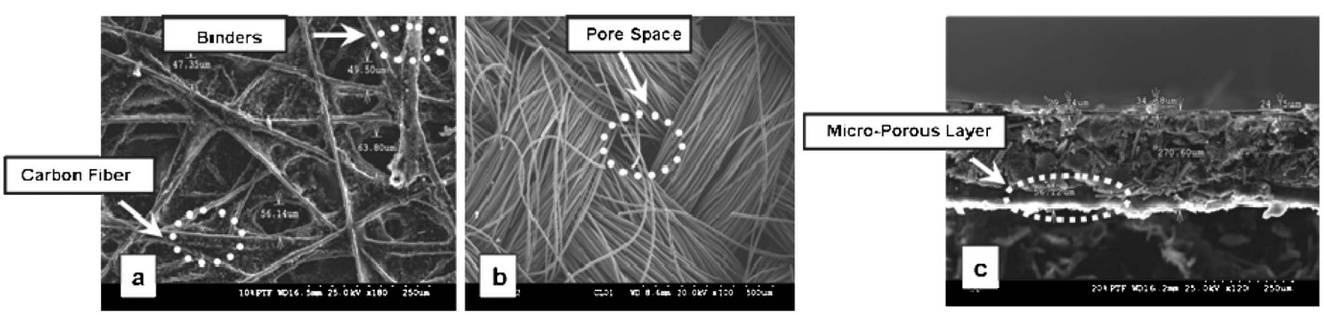

Figure 1. SEM images of (a) carbon paper, (b) carbon cloth, and (c) cross-sectional view of carbon paper with a microporous layer.

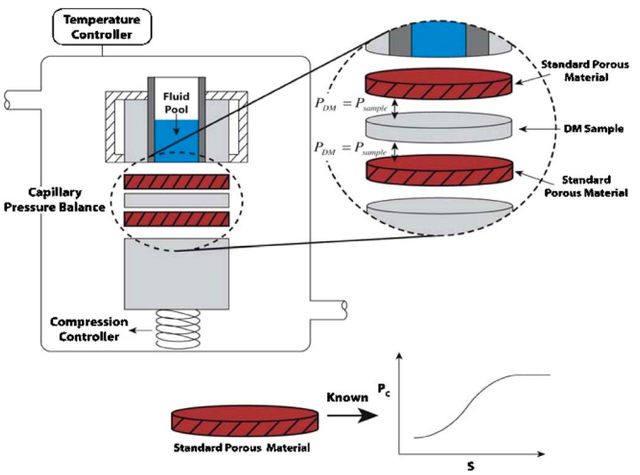

Figure 2. (Color online) Schematic view of the MSP technique.

Results and Discussion

Morphological characteristics.— The existence of bimodal pore distribution and nonuniform wettability bifurcate the transport paths of wetting and nonwetting phase, complicating the transport phenomena. Therefore it is necessary to first determine the full spectrum of dual-pore distribution of the bilayered DM.

The dual pore distribution (hydrophilic and total) of the DM samples is shown in Fig. 3. Three distinctive pore size ranges are observed for all DM samples. To distinguish the pore characteristics of the microporous layer and macroporous substrate, the pores are classified according to three classes, namely, macropores (pore diameter from 1 to 10 μm), mesopores (pore diameter from 0.1 to 1 μm), and micropores (pore diameter from 0.1 to 0.01 μm). Note that the classification of pore size is based on the current observation of pore distribution of the tested DM samples, and hence, it is different from the general criteria defined in soil science. The microporous layer generally consists of relatively smaller pores ranging from 100 to 500 nm, which can directly be identified from the measured pore distributions shown in Fig. 3. The average pore size of the DM samples ranges from 3.8 to 5.3 μm, indicating that the macropores dominate the entire structure, thus yielding an average open pore volume of 0.1 cm^3 for all samples, as shown in Table II. The total surface area per volume is found to vary from 13 to 30 m^2 cm^{-3}, and a significant difference is observed between the paper and cloth. The maximum surface area is observed in SGL 24CC (30 m^2 cm^{-3}), whereas the minimum one (13.2 m^2 cm^{-3}) is found for E-TEK Elat 1200W cloth. The existence of a high pore volume (i.e., high porosity) may indicate the possibility of higher transport of reactants to the catalyst layer, and thereby a higher limiting current density. However, high porosity is generally accompanied by excess water accumulation due to the low local capillary pressure. This, in turn, can hinder the effective reactant transport, causing significant decreases in cell performance.

In terms of hydrophilic pore characteristics, the range of pore size is broadly distributed between 1 and 10 μm, meaning that the microporous layer, which consists of micropores ranging from 0.1 to 0.01 μm, apparently contains considerably few hydrophilic pores and therefore can be treated as a completely hydrophobic substrate. This can be linked to the structural properties of the MPL. In fact, the microporous layer has a compact (small pores) and rigid structure compared to the ordinary DM, and it acts as a barrier to reduce local saturation and permit reactant gas diffusion to the catalyst layer. This compactness, rigidity, and high PTFE content of MPL provide a higher hydrophobic porosity.

The measured total porosity and hydrophilic porosity for all DM samples are tabulated in Table II. As seen in Table II, the hydrophilic

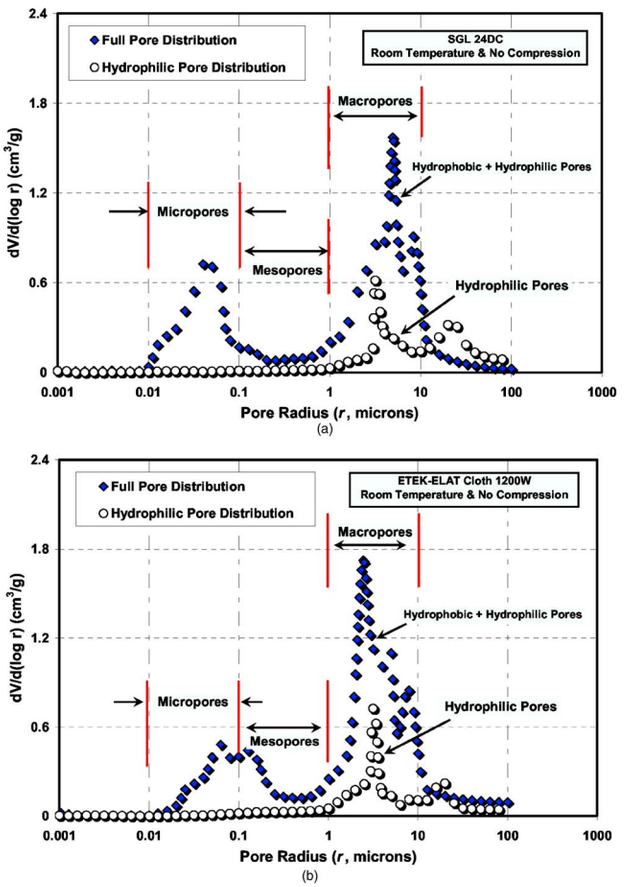

Figure 3. (Color online) Dual pore distribution of (a) SGL 24DC carbon paper and (b) E-TEK Elat 1200W carbon cloth

porosity is sensitive to the amount of PTFE loading and, as expected, shows a decreasing trend in response to an increase in the PTFE loading. The minimum hydrophilic porosity (0.16) is measured for E-TEK Elat 1200W carbon cloth, in which the PTFE content is greater than 20 wt % (the manufacturer does not publicly specify), whereas the maximum hydrophilic porosity (0.27) is observed for SGL 24BC with 5 wt % PTFE content.

Interconnected hydrophilic pores and water retention capacity.— The difference in DM morphologies leads to different mobile phase distributions. At a microscopic level, a pore surface will tend to imbibe the wetting phase while displacing the nonwetting phase.[23] Inside the pore, the wetting phase has a tendency to compress the nonwetting phase because of the high absorption of the wetting phase on the surface. In a *hydrophilic* DM pore, liquid water is the wetting phase (preferentially absorbed by the pore surface), whereas air (nonwetting phase) is compressed by the surrounding water. Due to the interfacial tensions at the interface, the gas (nonwetting) phase is displaced from the pore. While the nonwetting phase is transported in that manner, the displacement of the wetting phase requires a connected hydrophilic conduit or pathway because the isolated hydrophilic pore spaces mostly serve as the potential spots for the wetting phase to reside permanently. These isolated hydrophilic sites can only be occupied by water via condensation of the saturated water vapor because of the restricted access to these pores.

The water retention capacity (water storage), s_{wrc}, is a characteristic property of a fuel cell porous media and represents the available connected hydrophilic pore space of a fuel cell DM that can be spontaneously imbibed and occupied by liquid water. In fuel cell

Table II. Material properties of the tested DM determined by the MSP technique.[a]

Material	Total porosity	Hydrophilic porosity	Full pore volume (cm^3)	Total pore surface area (m^2/cm^3)	Hydrophilic pore volume (cm^3)
SGL 24BC (5% PTFE)	0.75,0.76	0.27	0.11	23.4	0.0408
SGL 24CC (10% PTFE)	0.76,0.76	0.17	0.11	30.0	0.0259
SGL 24DC (20% PTFE)	0.71,0.76	0.21	0.10	28.5	0.0287
ELAT 1200W (>20% PTFE)	0.72	0.16	0.12	13.2	0.0281

[a] Values from manufacturer technical specification sheets.

applications, the liquid water content stored (water retention capacity) in the DM during operation is critical for freeze/thaw, start-up, degradation, stability, and purging, because a higher residual water storage in a DM retards the thermal transients, causing additional damage during freeze/thaw. Furthermore, the excess stored water in DM can also act as a conduit for ionic impurities which facilitate the degradation rate of the electrode and electrolyte.[6] One approach to determine the potential water storage capacity (water retention capacity) of a DM is to isolate the connected hydrophilic pore network from the total network, because the detailed knowledge of the connected hydrophilic pore space would provide a reasonable estimate of the available pore space, in which the liquid water can occupy without any external force. To date, direct determination of the volume of the interconnected hydrophilic pore space has not been conclusively established, and to the best of the authors' knowledge, no truly direct values of the water retention capacity of a fuel cell DM as a function of DM material properties have been published.

One distinctive feature of the experimental approach (MSP) used in the present study is that the interconnected hydrophilic pore volume can be explicitly determined via spontaneous capillary imbibition tests. The spontaneous capillary imbibition is a natural process and requires existence of *interconnected hydrophilic pores*. During these imbibition experiments, the distilled water at the specified operating conditions (i.e., at room temperature under no compression) is imposed into the DM sample, which is located between two standard test specimens. The water imposed into the system is allowed to be imbibed by the available hydrophilic pores of the specimen assembly for a sufficient period of time until the system reaches the capillary equilibrium. Based on the amount of imbibition at each equilibrium, the corresponding capillary pressure-liquid saturation of the hydrophilic pore network and the available connected hydrophilic pore space are determined.[22] The same test procedure is employed for the other DM samples having different PTFE loadings. These measurements provide an appropriate estimation for the water retention capacity of the different DMs as a function of material properties, based on the accessible interconnected hydrophilic pore volume. In fuel cell operations, the water retention capacity represents the volume of water that would need to be removed by convection or evaporation forces, rather than naturally induced capillary drainage.

Capillary pressure vs water saturation of the connected hydrophilic pore network (excluding the isolated pores) was precisely measured for all the DM samples of interest. Figure 4a depicts the capillary pressure vs liquid saturation for SGL 24BC and SGL 24DC for the connected hydrophilic pore network. The capillary pressure curves follow the same trend for both cases but exhibit slight quantitative differences. The SGL 24BC treated with 5% PTFE content imbibes a maximum of 0.35 saturation ($s_{wrc} > 0.35$), whereas SGL 24DC tailored with 20% PTFE can only imbibe a maximum of 0.28 saturation ($s_{wrc} > 0.28$). Physically, this can be attributed to the fact that rendering the DM more hydrophobic decreases the total connected hydrophilic pathways, thus reducing the potential water retention capacity. In addition, the measured hydrophilic porosity of the SGL 24BC ($\varepsilon_{h\text{-philic}} = 0.27$) is greater than that of the SGL 24 DC sample ($\varepsilon_{h\text{-philic}} = 0.21$), which supports this physical reasoning. The estimated water retention capacities for tested DM samples are shown in Table III. It is worthwhile to emphasize that the water retention capacities of the tested DM samples given in Table III are higher than the total hydrophilic pore volume of the specimens listed in Table II. This may possibly stem from the exclusion of the volume of the pore throats in determination of hydrophilic pore volume. However, the determination of water retention capacity of the tested DM samples is based on the conduit or pathway volume that includes both the pores and the throats (passages between the pores).

A comparison of capillary pressure-saturation curves for SGL 24DC (20 wt % PTFE) carbon paper and E-TEK Elat 1200W (>20 wt % PTFE) carbon-cloth is shown in Fig. 4b. Despite the structural difference between a nonwoven paper and woven cloth, the capillary transport characteristics within the interconnected hydrophilic pores seem to follow a similar qualitative trend. However, a greater imbibition (maximum saturation of 0.28, $s_{wrc} > 0.28$) was observed in SGL 24DC tailored with 20 wt % PTFE, whereas the more hydrophobic E-TEK Elat 1200W carbon cloth can only imbibe up to a maximum saturation of 0.22 ($s_{wrc} > 0.22$), in reasonable agreement with the trend shown in Fig. 4a.

Note that these experiments were performed at room temperature and under no compression; therefore, the presented values are appropriate for the tested DM samples at this specified condition. However, the assembly compression and the operating temperature can lead to significant morphological changes in pore characteristics of the DM and are expected to strongly affect the capillary transport characteristics. Effects of these parameters are beyond the scope of this paper and are addressed in depth in the succeeding articles.[24,25]

Capillary transport characteristics of total pore network.— The difference in pressure across the interface between two immiscible fluids is referred to as the capillary pressure. The pressure difference is caused by the imbalance of the molecular forces at the phase interface (i.e., liquid and gas). It is proportional to the surface tension and inversely proportional to the effective radius of the interface. For a cylindrical pore, the capillary pressure can be represented by the Young–Laplace equation[26]

$$P_C = P_{nw} - P_w = \frac{2\gamma \cos\theta}{r} \quad [1]$$

where γ, θ, and r represent surface tension, contact angle, and pore radius, respectively. In order to measure the air-water capillary pressure-saturation curves of total hydrophobic pore network under drainage, additional experiments were performed. Highly wetting liquid octane was utilized as a working liquid to obtain the overall pore network capillary pressure curves as a function of liquid satu-

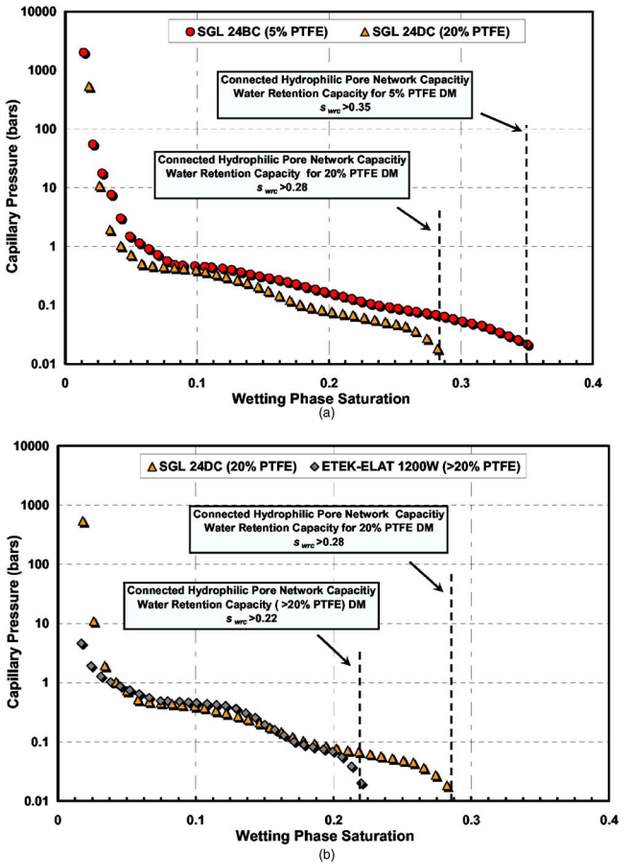

Figure 4. (Color online) Measured hydrophilic pore network capillary pressure vs wetting phase (water) saturation of (a) SGL 24BC and SGL 24DC, and (b) SGL 24DC and E-TEK Elat 1200W.

ration. The liquid saturation in the DM samples was measured at each capillary equilibrium condition and the corresponding equilibrium capillary pressure was recorded, based on the known capillary characteristics of the standard sample.[22] Octane capillary pressure-saturation data provide the necessary database for obtaining the capillary pressure-saturation curves of an air-water system.[20] The equivalent capillary pressure of a multiphase mixture in a specified pore can be calculated based on the Young–Laplace principle (Eq. 1) by converting the known capillary pressure of any known two phases occupying a pore having the same size to the equivalent water-air capillary pressure

$$r = \left(\frac{\gamma \cos \theta}{P_C}\right)_{\text{Oct}} = \left(\frac{\gamma \cos \theta}{P_C}\right)_{W} \quad [2]$$

The air-water capillary pressure of the total hydrophobic pore network as a function of nonwetting phase saturation for SGL 24 series is shown in Fig. 5. The individual curves follow similar trends; however, due to the different PTFE contents, the measured capillary pressure values differ slightly over the full liquid saturation spectrum. Three distinctive saturation regions are observed in the capillary pressure-saturation curves. At low saturations, especially $s_{nw} < 0.4$, the difference in measured capillary pressures between each DM is more pronounced. However, the discrepancy gradually diminishes as the saturation moves toward the moderate saturation region ($0.4 < s_{nw} < 0.7$). In the high-saturation region ($s_{nw} > 0.7$), the discrepancy between the three DM increases noticeably again. The shape of the measured capillary pressure-saturation curves is a result of the composite structure (i.e., the existence of MPL) of the tested DM samples, and the variations in the measured capillary pressure between each DM sample can be attributed to the differences in hydrophobic/hydrophilic pore volume because of the different amount of PTFE loadings in each DM sample. As shown in Fig. 5, the DM tailored with higher PTFE content exhibits a larger capillary pressure, especially for $s_{nw} < 0.4$. The highest capillary pressure is observed in SGL 24DC with 20% PTFE, whereas the lowest value at a given saturation is observed in SGL 24BC with 5% PTFE.

Table III. Water retention capacity of the tested DM samples.

Material	PTFE	Estimated water retention capacity
SGL 24BC	5	$s_{wrc} > 0.35$
SGL 24CC	10	$s_{wrc} > 0.30$
SGL 24DC	20	$s_{wrc} > 0.28$
ELAT 1200W	>20	$s_{wrc} > 0.22$

Figure 6 shows the capillary pressure vs PTFE content of the DM at different saturation values ($s_{nw} \leq 0.4$). At each saturation, a larger hydrophobic pore fraction (more hydrophobic media) corresponds to an increase in the measured capillary pressure. At high saturation ($s_{nw} = 0.4$), the increase in capillary pressure in response to the increase of the PTFE loading is relatively more severe (an increase of 0.21 bars from 5 to 20% PTFE) than those at lower saturations, $s_{nw} = 0.1$ (an increase of 0.075 bars from 5 to 20% PTFE). Physically, the surface adhesion force in carbon fibers is reduced by rendering the DM surface more hydrophobic, distorting the molecular force balance at the interface. As a result, the liquid water located on high PTFE loading fibers moves toward an unstable state, leading to a higher capillary pressure, which is consistent with the physical reasoning for enhanced liquid transport under high PTFE loading.[27]

Comparison of carbon cloth and paper.— To elucidate the structural difference of paper and cloth diffusion media substrates, the capillary pressure-saturation curves of SGL 24DC and E-TEK Elat 1200W carbon cloth are compared and shown in Fig. 7. Generally, carbon cloth and paper have different characteristics of spatial uniformity and degree of anisotropy. Carbon cloth has a spatially heterogeneous woven structure, resulting in three degrees of macroscopic anisotropy. In contrast, carbon paper is relatively more homogenous due to its random lacing, yielding two degrees of anisotropy.[7] Despite the existence of significant structural variations between these two types of DM, the overall capillary pressure curves for the hydrophobic pore network basically follow the same qualitative trend, even overlapping at moderate saturations and then deviating from each other at high saturation values, $s_{nw} = 0.55$ (Fig. 7). In terms of hydrophobicity, even though the exact PTFE content of E-TEK Elat 1200W carbon cloth is not publicly disclosed, both SGL 24DC and Elat 1200W cloth have similar PTFE contents (20% PTFE for SGL 24DC and >20% PTFE for E-TEK cloth), thereby yielding almost the same capillary pressure values over most of the saturation domain. Surprisingly, this observation suggests that the PTFE content, especially at moderate saturations ($s_{nw} < 0.5$), is a more dominating factor affecting the capillary pressure curves, rather than the types of DM base material.

Effect of a microporous layer.— When the capillary pressure curve for each DM is analyzed, a dramatic increase in capillary pressure is noticeable at high threshold saturations ($s_{nw} > 0.7$). This sudden increase in capillary pressure is a result of the microporous layer. Gostick et al.[20] reported that the existence of a microporous layer can be extracted independently from the capillary pressure curves and pore size distribution. The pore size distribution of the tested DM samples yielded evidence of the existence of bilayered DM, which is addressed in the previous section. The region showing evidence of the microporous layer in these datasets is shown in Fig. 8. The significant increase in capillary pressure at high saturation ($s_{nw} > 0.7$) can be linked to the compact structural characteristics of a microporous layer. Typically, microporous layers have a packed

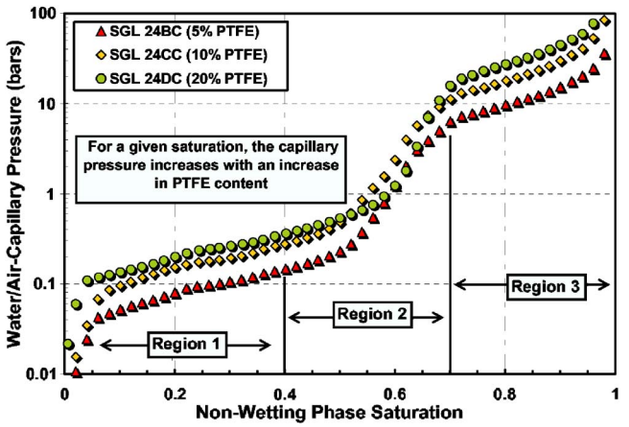

Figure 5. (Color online) Measured drainage capillary pressure vs nonwetting phase saturation for the hydrophobic pore network of the tested SGL 24 series carbon paper DM samples.

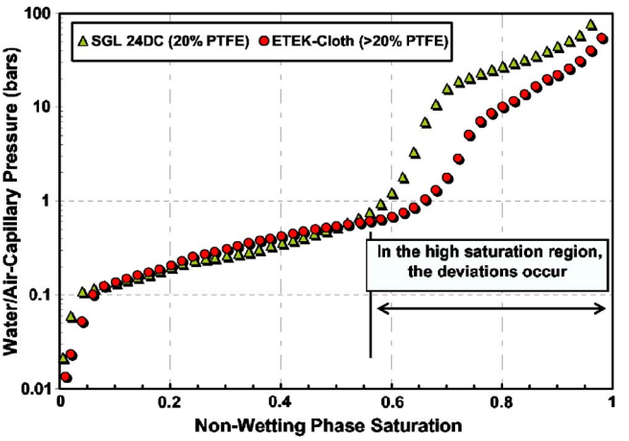

Figure 7. (Color online) Measured drainage capillary pressure vs nonwetting phase saturation for the hydrophobic pore network of the tested SGL 24DC carbon paper and E-TEK Elat 1200W cloth.

(small pores) and rigid structure, thus requiring higher capillary pressure to overcome the surface energy of the diminutive and highly hydrophobic pores of the MPL. It is important to note that the high capillary pressure measured at high saturations ($s_{nw} > 0.7$) for these tested composite materials (macro DM substrate and MPL) is a result of the highly hydrophobic MPL. These measurements indicate that in fuel cell operations, the pores of the MPL would possibly remain open due to the high pore resistance, while the macro DM substrate completely floods.

Leverett approach.— Standard Leverett J-function.— One common approach currently used in macroscopic modeling studies for predicting the fluid distribution profiles in porous media is the direct implementation of an empirical constitutive correlation describing the capillary pressure as a function of liquid saturation. Several empirical and semiempirical expressions are available which attempt to describe the behavior of capillary pressure in terms of porous media and fluid properties. The traditional Leverett approach proposed by Leverett[9] and Udell[10] has been widely adopted by the fuel cell community. Leverett[9] suggested a semiempirical approach using dimensional analysis to represent the capillary pressure-saturation behavior of the porous media in the following nondimensional form

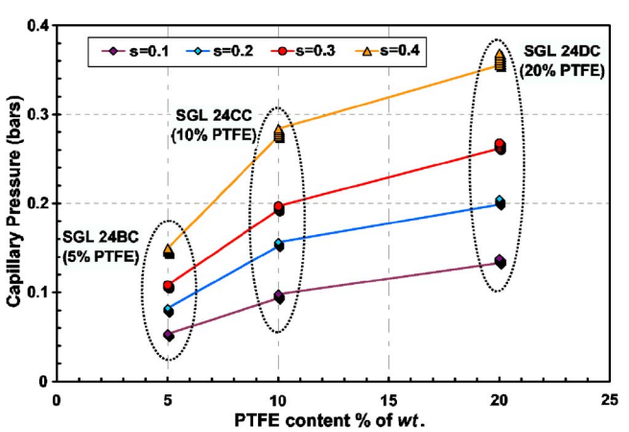

Figure 6. (Color online) Measured drainage capillary pressure vs PTFE wt % at specified saturations for SGL 24 series DM samples.

$$\frac{P_C}{\gamma}\left(\frac{k}{\varepsilon}\right)^{1/2} = f(s) \qquad [3]$$

where P_C, γ, k, ε, and s are capillary pressure, surface tension, permeability, porosity of the porous media, and liquid saturation, respectively. Based on this empirical description (Eq. 3), Udell[10] introduced a contact angle term for scaling capillary drainage curves and proposed the following functional form of $f(s)$, or so-called Leverett J-function $[J(s)]$ to correlate the capillary pressure as a function of saturation and relevant transport properties of porous media (i.e., porosity and permeability)

$$J(s) = 1.417(1 - s) - 2.120(1 - s)^2 + 1.263(1 - s)^3 \qquad [4]$$

The Leverett J-function given in Eq. 4 is deduced using the experimental data obtained by Leverett[9] for a range of common soils with uniform wettability. In terms of modeling the capillary transport in fuel cell diffusion media, Pasaogullari and Wang[11] and Nam and Kaviany[12] proposed an extension version of Leverett J-function to account for the hydrophobicity characteristics of the porous media by adjusting the saturation term "$(1 - s)$" in the original Udell's correlation with the term "s" (liquid saturation) for hydrophobic media (i.e., $\theta > 90°$)

$$P_C = \gamma \cos\theta\left(\frac{\varepsilon}{k}\right)^{1/2} J(s)$$

$$J(s) = \begin{cases} 1.417(1 - s) - 2.120(1 - s)^2 + 1.263(1 - s)^3 & \text{if } \theta < 90° \\ 1.417s - 2.120s^2 + 1.263s^3 & \text{if } \theta > 90° \end{cases} \qquad [5]$$

The contact angle represents the degree of the wettability of the porous media (i.e., $\theta < 90°$ hydrophilic media and $\theta > 90°$ hydrophobic media). Even though the standard Leverett approach equipped with J-function given in Eq. 5 represents a useful starting point toward achieving an accurate two-phase transport model in fuel cells studies, the origin of this approach does not precisely represent the complex heterogeneous structure of fuel cell diffusion media.[28] For instance, the traditional Leverett approach (Eq. 5) is capable of incorporating the effects of interfacial tension but uses a simple relation for the average pore radius $(k/\varepsilon)^{0.5}$, essentially neglecting the tortuous nature of fuel cell porous media.[29] Even though the J-function satisfactorily correlates data from unconsolidated sands and sandstones having uniform formation, it is limited in its ability to describe the capillary characteristics of the porous media

when the porous media of the interest exhibits a great deal of heterogeneity or mixed wettability, such as that occurring in fuel cell porous DM.[29]

Empirical function for SGL 24 series fuel cell DM, $K(s_{nw})$.— The capillary pressure-saturation curves for the tested SGL 24 series DM samples were used as a benchmark data to compile an expanded database. This database was then utilized to deduce an appropriate empirical nondimensional correlation describing the capillary pressure as a function of PTFE content and liquid saturation. A multidimensional linear regression model was employed to precisely correlate the capillary pressure with the relevant nondimensionalized experimental parameters. A total of 3200 experimental data points were processed and integrated into the computational database to determine the best polynomial fit. The nature of the capillary pressure-saturation curves exhibits a continuous "S" shape, yielding four inflection points. In order to improve the precision of the empirical correlation and eliminate the potential uncertainty associated with the complex shape of the capillary pressure-saturation curves, the overall saturation domain was divided into three regions and three continuous empirical fits were deduced based on the experimental data corresponding to these three regions, namely, $0 < s_{nw} < 0.50$ (less hydrophobic region), $0.50 \leq s_{nw} \leq 0.65$ (transition region or relatively more hydrophobic region), and $0.65 < s_{nw} < 1.00$ (high capillary pressure region due to the existence of a hydrophobic, microporous layer). The final form of the characteristic Leverett function, $K(s_{nw})$, for the tested SGL 24 carbon paper series is found as

$$P_C = \gamma\left(\frac{\varepsilon}{k}\right)^{1/2} K(s_{nw}) \quad [6]$$

$$K(s_{nw}) = \begin{cases} \text{wt \%}(0.0469 - 0.00152(\text{wt \%}) - 0.0406s_{nw}^2 + 0.143s_{nw}^3) + 0.0561 \ln s_{nw} & 0 < s_{nw} < 0.50 \\ \text{wt \%}(1.534 - 0.0293(\text{wt \%}) - 12.68s_{nw}^2 + 18.824s_{nw}^3) + 3.416 \ln s_{nw} & 0.50 \leq s_{nw} \leq 0.65 \\ \text{wt \%}(1.7 - 0.0324(\text{wt \%}) - 14.1s_{nw}^2 + 20.9s_{nw}^3) + 3.79 \ln s_{nw} & 0.65 < s_{nw} < 1.00 \end{cases}$$

where wt % and s_{nw} represent PTFE weight percentage in the DM and nonwetting saturation, respectively. The normal plot of residuals, the histogram of residuals, chart of residuals, and residuals vs fits were performed in order to check the validity of the presented empirical correlation (i.e., homogeneity of variance, nonindependence of variables, normality) as well as to detect outliers in experimental data. The approximation in the prescribed functional form provided a close fit to the experimental data.

The key feature of the presented empirical fit in Eq. 6 is that the connection between the liquid saturation and the mixed wettability characteristics of the DM is precisely linked to the capillary pressure. Adjusting the PTFE variable (wt %), which is acting in parallel with other parameters, enables successful determination of the capillary pressure as a function of hydrophobic additive loading of the DM.

Due to the pore level experimental limitations, external contact angle measurements are one common approach employed to estimate a statistical average of contact angles associated within the highly heterogeneous pores of DM,[30] although the appropriateness of this approach has been questioned.[30] Such external contact angle measurements on DM surface may provide quantitative estimations of the average internal contact angle, but these measurements fail to include the effects of the different levels of surface energy associated with the carbon fibers, therefore ignoring the mixed wettability characteristics of DM. One distinctive feature of the present empirical correlation (Eq. 6) is that no contact angle parameter is required as an input, because the PTFE parameter (wt %) accounts for the anisotropic nature of the hydrophobic coating of the DM. However, surface tension, a significant parameter relating the interaction of the flowing fluid and carbon fibers, is included in the present Leverett function (Eq. 6) as an input parameter. Porosity and permeability, the governing transport parameters of the DM, are also retained in the new approach (Eq. 6) as it is in the original Leverett and Udell formulation (Eq. 5).

Validation, comparison, and limitations.— Figures 9 and 10 compare the predicted capillary pressure by using both the present Leverett function, $K(s_{nw})$, and the standard Leverett function, $J(s_{nw})$, with respect to the actual experimental capillary pressure data for SGL 24BC and SGL 24DC DM samples. As clearly seen from these figures, the present empirical function predicts the measured capillary pressures well, especially for $s_{nw} < 0.5$, whereas the standard Leverett function exhibits an enormous deviation from the experimental data over the entire saturation domain, especially at high saturations (more than 100% off). At moderate saturations such as $0.5 < s_{nw} < 0.6$, the empirical fit deviates slightly from the experimental data to capture the inflection point of the capillary pressure curve trend. However, in the high-saturation region ($s_{nw} > 0.6$), the deviation is reduced and the present Leverett-type empirical function $[K(s_{nw})]$ precisely predicts the capillary pressure. The significant difference between approximation of the standard Leverett function $[J(s_{nw})]$ and experimental data strongly suggests that the standard Leverett function is ineffective for describing the capillary transport characteristics of the fuel cell DM, as also previously addressed in Ref. 1. Note that in these comparisons, the contact angle term ($\cos\theta$) originally given in Udell's correlation (Eq. 5) has been assumed to be one in order to perform the comparison with the maximum possible value of the capillary pressure that can be predicted by using the standard Leverett approach given in Eq. 5. The predicted capillary pressure values by the traditional approach considerably underpredicts the measured capillary pressure. Thus the use of any other contact angle value will result in a reduced capillary pressure prediction, and the departure from the measured data will be even greater than shown in Fig. 9 and 10.

The physical reason underlying the significant deviation between the standard *J*-function and experimental data may stem from the fact that even though, at a minute length scale, the DM has a similar geometrical structure with the common type of soils, the magnitude of characteristic transport properties, including the grain size, pore radius, and relative permeability, is relatively smaller in fuel cell DM. Furthermore, the DM is highly heterogeneous and anisotropic with a low volume-to-surface-area ratio, unlike the soils used in the original derivations (Eq. 4 and 5). The uniqueness of the empirical function $[K(s_{nw})]$ presented in this study is that it accounts for the nonuniform wettability characteristics associated with the nature of the fuel cell DM and it relies on the actual benchmark capillary pressure data for a range of fuel cell DM tailored with various PTFE loadings. Therefore it provides an accurate prediction of capillary pressure in terms of liquid saturation and PTFE content under no compression and at room temperature. As seen from Fig. 11, the present Leverett-type empirical function $[K(s_{nw})]$ can accurately capture the effects of PTFE content on capillary pressure over the entire saturation spectrum by resolving the change in interfacial surface energy associated within the pores for the paper-based DM.

Recognizing the fact that the present polynomial fit (Eq. 6) was

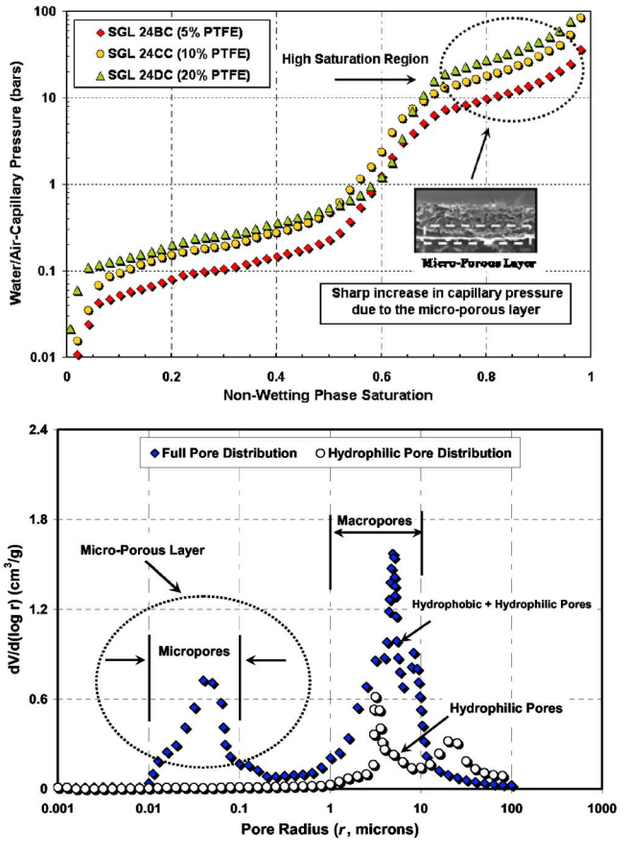

Figure 8. (Color online) Identification of the microporous layer from the measured capillary pressure-saturation curves and dual-pore distribution.

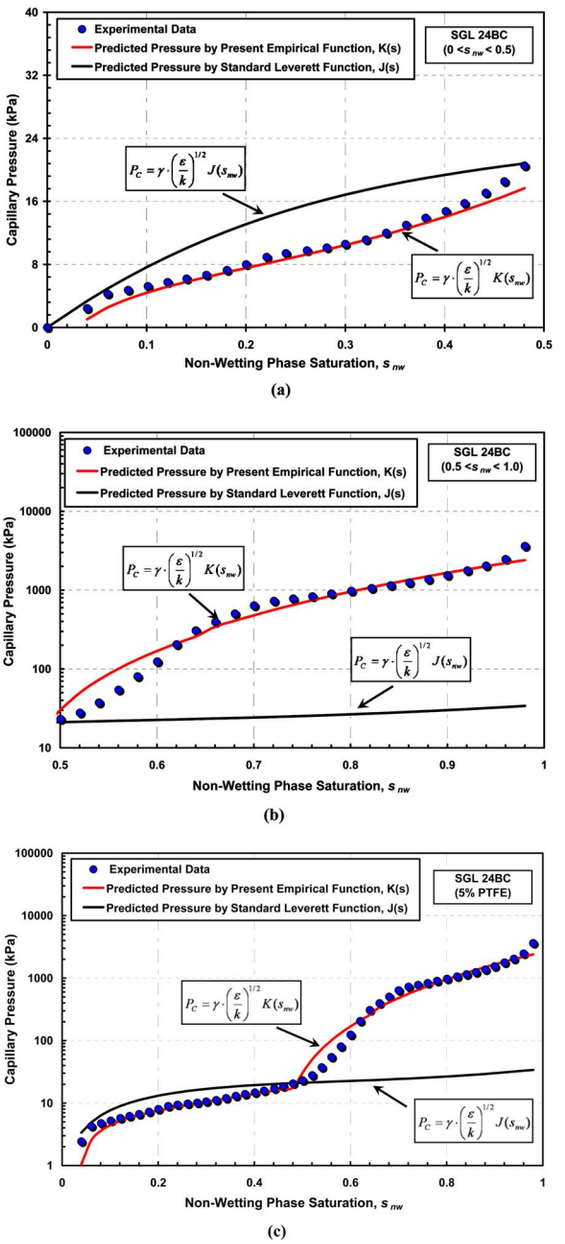

Figure 9. (Color online) Comparison of the new Leverett-type empirical function (Eq. 6), the standard Leverett function, and the experimental data for SGL 24BC (5% PTFE) over a saturation range of (a) $0 < s_{nw} < 0.5$, (b) $0.5 < s_{nw} < 0.1$, and (c) $0 < s_{nw} < 1$.

derived purely based on the experimental data for SGL 24 carbon paper series coated with MPL, the applicability of the empirical fit (Eq. 6) to a carbon cloth DM with MPL needs to be addressed. To assess the prediction accuracy of the present Leverett-type empirical function $[K(s_{nw})]$, the predicted capillary pressure (by Eq. 6) of E-TEK Elat 1200W carbon cloth was compared with the experimental data. The material properties of E-TEK Elat 1200W carbon cloth were directly integrated into the capillary pressure correlation given in Eq. 6, and the capillary pressure vs saturation is shown in Fig. 12. Although the exact PTFE loading of E-TEK cloth is not publicly disclosed, a reasonable value of 20% PTFE is assumed depending upon the known PTFE range of E-TEK cloth (>20 wt % PTFE). As seen from the Fig. 12, the present empirical function successfully approximates the capillary pressure up to saturation 0.5. After that point, as the saturation increases gradually, the predictions tend to exhibit a deviation from the experimental data, however, with diminishing significance. This could be the result of nonuniform PTFE distribution in the cloth material. The vast deviation associated with the standard Leverett function, $J(s_{nw})$, is more pronounced and much greater over the entire region, again demonstrating the ineffectiveness of the standard Leverett function to predict the capillary characteristics of any type of fuel cell DM.

Limitations.— In terms of limitations, the final form of the present empirical fit given in Eq. 6 is deduced from the drainage capillary pressure-saturation measurements of SGL 24 series composite carbon paper DM (coated with MPL), including SGL 24BC (5 wt % PTFE), SGL 24CC (10 wt % PTFE), and SGL 24DC (20% PTFE). Therefore the present approach is applicable for the tested DM samples within the limits of testing conditions. For developing a more generalized approach, additional benchmarking of different DM samples needs to be performed to expand the database. The present correlation given in Eq. 6 is derived based on the generated data for the DM samples coated with a microporous layer. Therefore, the porous media of interest herein is a composite structure. The capillary pressure-saturation curves of the DM macrosubstrate (without MPL) can be extracted from the overall behavior of the composite structure by using the corresponding the pore size distribution and porosities of the macro- and microsubstrate (MPL), as also discussed in Ref. 20. In other words, the characteristic capillary pressure-saturation relationship of the macro-DM substrate (i.e., without MPL) can be determined from the given composite relationship in Eq. 6 by extending the capillary pressure-saturation trend of the composite DM from low saturation to high saturation, i.e., eliminating the MPL region. (For example, to predict the behavior in the macro-DM alone for SGL 24 series, the empirical Leverett-type

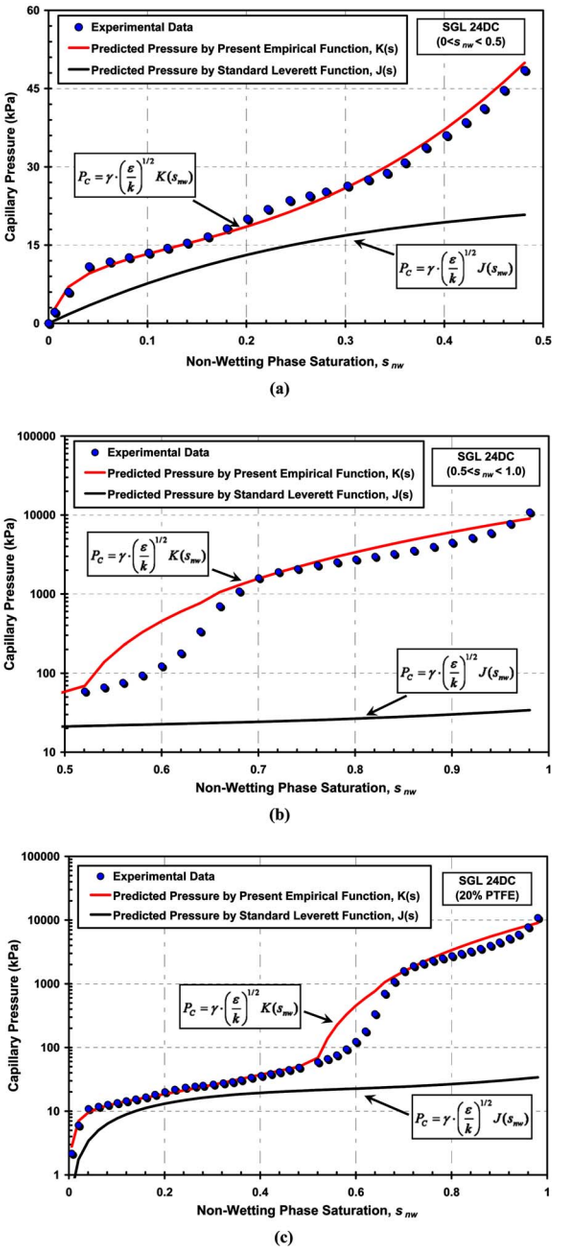

Figure 10. (Color online) Comparison of the new Leverett-type empirical function (Eq. 6), the standard Leverett function, and the experimental data for SGL 24DC (20% PTFE) over a saturation range of (a) $0 < s_{nw} < 0.5$, (b) $0.5 < s_{nw} < 0.1$, and (c) $0 < s_{nw} < 1$.

function, $K(s_{nw})$, given for the saturation range $0 < s_{nw} < 0.5$, can be extended to $0 < s_{nw} < 1$.) In this way, the empirical function for the macro DM region alone (without MPL) can be estimated before specific experimental data for these materials become available.

Conclusion

For the first time, a validated Leverett-type empirical function appropriate for SGL 24 carbon paper series fuel cell DMs coated with MPL was developed to describe the capillary pressure-saturation relationship of this series of DM samples. The benchmark data were generated from the direct measurements of drainage capillary pressure-liquid saturation curves for DMs tailored with PTFE content ranging from 5 to 20 wt %. The expanded database was

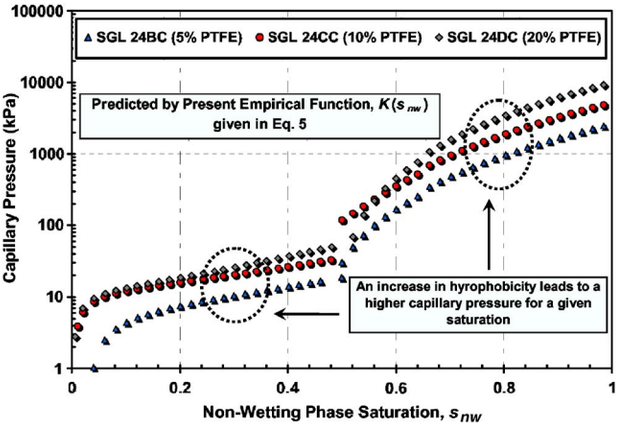

Figure 11. (Color online) Predicted capillary pressure by the empirical fit given in Eq. 6 vs nonwetting saturation for SGL 24 carbon paper series treated with different PTFE loadings.

utilized to deduce a unique empirical fit that precisely correlates the capillary pressure as a function of nonwetting saturation and PTFE content of the DM. A detailed comparative analysis of the present Leverett function and the standard Leverett function was performed. The empirical function accurately predicts the measured capillary pressures in almost the entire saturation range ($0 < s_{nw} < 1$), whereas the standard Leverett function exhibits a large deviation (more than 100%) from the experimental data, especially at high saturation ($s_{nw} > 0.5$). In addition, the empirical fit given in Eq. 6 predicts the measured capillary pressure of E-TEK Elat 1200W carbon-cloth DM reasonably well compared to the standard Leverett approach, supporting the effectiveness of the new approach.

A key advantage of the presented empirical function over the standard Leverett function is that it can successfully incorporate the rigorous interaction of liquid saturation and DM material properties; thus, it is capable of accounting for the structural heterogeneity associated with the nature of the fuel cell DM. Furthermore, it can implicitly resolve the change in internal contact angle caused by the anisotropic nature of the hydrophobic coating, eliminating any ambiguity regarding the need for selection of a representative contact angle.

The presented correlation and experimental data were generated at room temperature and under no compression. However, due to the various operational conditions, DM can be subjected to different

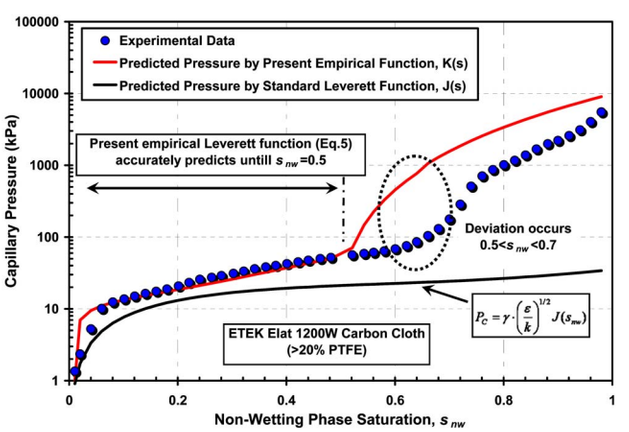

Figure 12. (Color online) Comparison of the present Leverett-type empirical function, the standard Leverett function, and the experimental data for E-TEK Elat 1200W cloth.

temperatures and different compressions, causing a significant change in the capillary transport characteristics. The effects of compression and temperature deserve deeper examination to further isolate the impact of these effects on transport characteristics and are the subject of succeeding publications.[24,25] For now, the presented empirical function represents an improvement in precision of PEFC DM multiphase transport predictions.

Acknowledgments

This research is supported by National Science Foundation grant no. CTS-0414319. The authors thank to Dr. Alex Sakars from Porotech, Ltd., for performing the MSP experiments and Elise Corbin for her help during the preparation of Fig. 2.

The Pennsylvania State University assisted in meeting the publication costs of this article.

List of Symbols

k	permeability, m^{-2}
P	pressure, N m^{-2}
s	saturation, unitless

Greek

ε	porosity, unitless
θ	contact angle, degree
γ	surface tension of water-air, N m^{-1}

Subscripts

c	capillary
g	gas
irr	irreducible
l	liquid
w	wetting phase
nw	nonwetting phase
wrc	water retention capacity

References

1. E. C. Kumbur, K. V. Sharp, and M. M. Mench, *J. Power Sources*, **168**, 156 (2007).
2. T. V. Nguyen and M. W. Knobbe, *J. Power Sources*, **114**, 70 (2003).
3. A. Z. Weber and J. Newman, *Chem. Rev. (Washington, D.C.)*, **104**, 4679 (2004).
4. A. Kraytsberg and Y. Ein-Eli, *J. Power Sources*, **160**, 194 (2006).
5. F. Y. Zhang, X. G. Yang, and C. Y. Wang, *J. Electrochem. Soc.*, **153**, A225 (2006).
6. J. J. Kowal, A. Turhan, K. Heller, J. Brenizer, and M. M. Mench, *J. Electrochem. Soc.*, **153**, A1971 (2006).
7. S. Litster and N. Djilali, in *Transport Phenomena in Fuel Cells*, B. Suden and M. Faghri, Editors, 1st ed., Chap. 5, WIT Press, Ashurst, U.K. (2006).
8. U. Pasaogullari and C. Y. Wang, *Electrochim. Acta*, **49**, 4359 (2004).
9. M. C. Leverett, *Trans. Am. Inst. Min., Metall. Pet. Eng.*, **142**, 152 (1941).
10. K. S. Udell, *Int. J. Heat Mass Transfer*, **28**, 485 (1985).
11. U. Pasaogullari and C. Y. Wang, *J. Electrochem. Soc.*, **151**, A399 (2004).
12. J. H. Nam and M. Kaviany, *Int. J. Heat Mass Transfer*, **46**, 4595 (2003).
13. T. V. Nguyen, *J. Electrochem. Soc.*, **143**, 103 (1996).
14. E. Antolini, L. Giorgi, and A. Pozio, *Mater. Sci. Technol.*, **13**, 65 (1998).
15. M. V. Williams, E. Begg, L. Bonville, H. R. Kunz, and J. M. Fenton, *J. Electrochem. Soc.*, **151**, 1173 (2004).
16. J.-H. Jang, W.-M. Yan, and C.-C. Shih, *J. Power Sources*, **161**, 323 (2006).
17. Escribano, S., Blachot, J.-F., Etheve, J., Morin, A., and Mosdale, R., *J. Power Sources*, **156**, 8 (2006).
18. H.-K. Lee, J.-H. Park, D.-Y. Kim, and T.-H. Lee, *J. Power Sources*, **131**, 200 (2004).
19. M. Prasanna, H. Y. Ha, E. A. Cho, S. A. Hong, and I. H. Oh, *J. Power Sources*, **131**, 147 (2004).
20. J. T. Gostick, M. W. Fowler, M. A. Ioannidis, M. D. Pritzker, Y. M. Volfkovich, and A. Sakars, *J. Power Sources*, **156**, 375 (2006).
21. N. Djilali, *Energy*, **32**, 269 (2007).
22. Y. M. Volfkovich, V. S. Bagotzky, V. E. Sosenkin, and I. A. Blinov, *Colloids Surf., A*, **187-188**, 349 (2001).
23. J. Bear, *Dynamics of Fluids in Porous Media*, Chap. 9, p. 441, Dover Publications, Inc., New York (1972).
24. E. C. Kumbur, K. V. Sharp, and M. M. Mench, *J. Electrochem. Soc.*, **154**, B1305 (2007).
25. E. C. Kumbur, K. V. Sharp, and M. M. Mench, *J. Electrochem. Soc.*, **154**, B1315 (2007).
26. T. A. Corey, *Mechanics of Immiscible Fluids in Porous Media*, 1st ed., Water Resource Publications, Highlands Ranch, CO (1994).
27. E. C. Kumbur, K. V. Sharp, and M. M. Mench, *J. Power Sources*, **161**, 333 (2006).
28. H. Ohn, T. V. Nguyen, D. Jacobson, D. Hussey, and M. Arif, *ECS Trans.*, **1**(6), 481 (2006).
29. A. A. Garrouch, *Energy Fuels*, **13**, 1021 (1999).
30. V. Gurau, M. J. Bluemle, E. S. De Castro, Y.-M. Tsou, J. A. Mann, and T. A. Zawodzinski, Jr., *J. Power Sources*, **160**, 1156 (2006).